Scaling behavior of diffusion on binary Archimedean random electrical lattices and on layers

J-M Teissier[1*] and S Russ[1]
[1] *Institut für Theoretische Physik, Arnimallee 14, Freie Universität Berlin, 14195 Berlin, Germany*
(Dated: March 2, 2020)

We investigate the diffusion and conductance behavior of binary Archimedean lattices and binary layer systems (with bonds of conductances G_A and G_B between the sites) close to the percolation threshold (of the G_A-lattice) by numerical simulations and by scaling theories. We are interested in possible influence factors of geometry, defects and thickness on the conductivity and in particular on the critical exponents of the phase transition between insulating and conducting phases. We aim for information that will help to decide if experimentally observed transitions between good and poor conductors are due to percolation effects, even if in real experiments, the pure theoretically expected behavior is often not exactly reproduced. We find that the Archimedean lattices of all kinds show the expected universal behavior in high precision. Layer systems show a crossover from $2D$ to $3D$ behavior that becomes visible beyond a certain layer thickness. We discuss by which processes the universal behavior might be disturbed.

PACS numbers: 64.60.ah,89.75.Da,72.80.Ng

I. INTRODUCTION

The percolation model [1, 2] is well-known for its ability to describe a phase transition between an insulating and a conducting phase and has among others been used to describe insulator-conductor transitions in electrolytes [3], two-component conductors [4–6], binary glasses and gas sensors [7–9]. However, the universal critical exponents of the percolation transition have so far numerically only been tested on idealized square or cubic lattices [4–6], while data on other geometries or on systems with defects, finite-size effects, surface reconstructions and others are surprisingly rare. To see if an experimentally observed transition, such as the transition from an insulator to a conductor, is really due to percolation effects, it would, however, be of high interest to know in more detail which kinds of changes as compared to the standard behavior may occur beyond perfect and square or cubic lattices.

In practice, one normally compares the experimentally observed properties to the ones of mathematical percolation. As one recent example, the percolation transition has been used in the context of gas sensing, when exposing a surface of interconnected semi-conducting grains to air with increasing gas concentration [7, 9–12]. Due to chemical processes between the gas particles and the grain surfaces, a certain number of grains drastically increase their conductivity, which leads to a sudden and dramatic increase of the conductivity of the whole system. This has been interpreted in the framework of the percolation model, even if the values of the observed exponents deviated from the well-known exponents of percolation theory [11, 12].

In this paper, we therefore want to take a closer look at the phenomena at the percolation transition. First, we perform numerical tests of the conductivity exponent and the related scaling behavior on many different idealized, but non-square lattice geometries. Second, we investigate systems of layers that are somehow between two and three dimensions. As the universal exponents do depend on the dimension, layers must experience some change of the critical exponents when increasing the layer thickness. We believe that this work will give valuable hints for the interpretation of conductivity transitions in real materials.

We concentrate on the bond percolation model, where one starts with an empty lattice and chooses a bond occupation probability p. A portion p of all nearest-neighbor connections are randomly occupied by bonds G_A, while all other nearest-neighbor connections are occupied by bonds G_B (with probability $q = 1 - p$). Following the notation of [4], we describe the conductivity of these systems as $\sigma(p, G_A, G_B)$. In "standard percolation", only connecting and broken bonds exist, $G_A = 1$, $G_B = 0$. More interesting are "binary mixtures" with two types of conducting bonds, where $h = G_B/G_A$ and $0 < h < 1$. This case is called a "Random Resistor Network" (RRN), when $G_A = 1$, $G_B \ll 1$ and a "Random Superconducting Network" (RSN) when $G_B = 1$, $G_A \gg 1$ [6]. To apply this model to conductivity problems ("electrical percolation"), G_A and G_B are considered as conductances between two nodes of an electrical network.

In standard percolation, the network is conducting only when a continuous path of conductances G_A connects two opposite sides of the lattice, forming the so-called "infinite cluster". When the lattice size goes to infinity, the transition between the insulating and the conducting phase takes place at a well-defined (and well explored) occupation probability $p = p_c$ that is therefore

*Present address: Technische Universität Berlin, ER 3-2, Hardenbergstr. 36a, 10623 Berlin, Germany

named the "critical probability". The value of p_c is non-universal, i.e. it depends not only on the dimension d, but also on the considered lattice geometry and the type of percolation (e.g. site or bond percolation).

An RRN network, on the other hand, is weakly conducting already at small values of p. Approaching p_c from below, the conductivity increases rapidly from the one of a pure G_B-network to the one of a G_A-network. Scaling theories describe the range around $p = p_c$, $h = 0$, when both values are varied. Clearly, both types of changes (p as well as h) may be relevant in experimental situations.

The paper is organized as follows: In section 2, we summarize the important concepts about random walks on percolation systems that we use in the following, while in section 3, we describe our numerical methods. In sections 4, we present our numerical results and the corresponding scaling theories on perfect Archimedean lattices. In section 5, we investigate layers that are between $d = 2$ and $d = 3$ to enforce a change of the values of the critical exponents. A summary and conclusions are given in section 6.

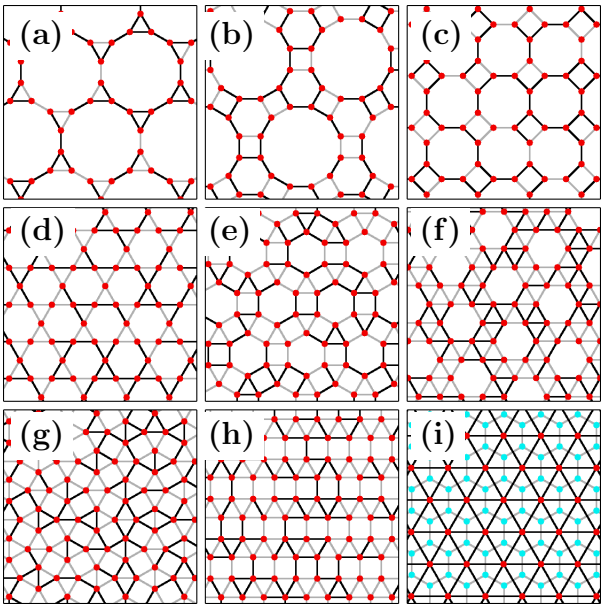

FIG. 1: [Color online] Ten out of eleven Archimedean lattices (without the Square lattice (□)) at their respective percolation thresholds where black lines stand for G_A bonds and gray lines for G_B bonds. The symbols in bracket are the ones used in the figures for the respective geometry (see also Tab. I). (a) 3-12 (3), (b) Cross (+), (c) Square octagon (◇), (d) Kagome (K), (e) Rhombitrihexagonal (R), (f) Snub hexagon (also called "Maple Leaf" - M), (g) Snub square (also called "Puzzle" - P), (h) Frieze (F) (i) Honeycomb (H) (cyan dots) and triangular (△) lattice (red dots), showing that they are dual to each other.

II. SCALING RELATIONS OF ELECTRICAL PERCOLATION

The electrical conductivity $\sigma = nq\mu_e$ (with the density n of charge carriers of charge q and mobility μ_e) can be determined via the Einstein relation $\mu_e = qD/(k_BT)$ with the temperature T, the Boltzmann constant k_B and the diffusion coefficient D, where D is accessible via random walk simulations [1]. Therefore, to determine σ, we perform random walks on the given lattices and calculate the mean squared displacement $\langle r^2(t)\rangle$ where $r(t)$ is the distance that the walker has traveled after t units of time (number of time steps). For $h = 0$ (standard percolation in the RRN case) and for p slightly above criticality, the system is self-similar for length-scales below the correlation length ξ that decreases with increasing values of p. The self-similarity of the lattice considerably slows down the diffusion process and leads to "anomalous diffusion", where $\langle r^2(t)\rangle$ is not proportional to t. When the walker reaches a distance beyond ξ from its starting point, $r(t) > \xi$, "normal diffusion" occurs, where the self-similar structure of the system does no longer dominates the diffusion behavior. When t is sufficiently large, $\langle r^2(t)\rangle$ always becomes linear in time for $p \neq p_c$ or for $G_B > 0$. For the simulations, we translate the conductivities G_A or G_B of the resistive network into jump frequencies along the respective bonds (see also section III) and determine $D \equiv \lim_{t\to\infty}\langle r^2(t)\rangle/t$ (where for simplicity, the usual prefactor $1/(2d)$ with the dimension d has been set to unity).

Figure 1 shows one class of lattices that we consider in this work, the so-called "Archimedean lattices". Archimedean lattices are ordered lattices, where all bond lengths are equal and all vertices are surrounded by the same polygons (e.g. by four squares in a square lattice or by one square and two octagons in the case of the square octagon lattice). There exist eleven Archimedean lattices, which are also called uniform tilings [13]. The values of p_c for site and bond percolation can be found in [13] and [14], respectively (and in the references therein), but to the best of our knowledge, no simulations of $\langle r^2(t)\rangle/t$ on these lattices have yet been performed.

In the following, we shortly describe several helpful relations that apply in the scaling regimes, i.e. for small values of $|p - p_c|$ and for $h \ll 1$ in the RRN case and for $h \gg 1$ in the RSN case. We hereby assume that the charge density n does not depend on h, so that we can treat D and σ in similar ways. For $h = 0$ and $p > p_c$, close to p_c (RRN case), the behavior of σ, D and n depends on $(p-p_c)$ by similar power-laws [1], i.e. $\sigma \propto (p-p_c)^{\mu}$, $D \propto (p-p_c)^{\mu'}$ and $n \propto (p-p_c)^{\beta}$ with well-known universal exponents μ and β and $\mu' = \mu - \beta$. For $h \to \infty$ (RSN case) and close to criticality, one observes a very similar power-law behavior $\sigma \propto (p_c - p)^{-s}$ for $p < p_c$, close to p_c with the critical exponent s. For $p = p_c$, on the other hand, we have

$$\sigma \propto D \propto h^u, \tag{1}$$

where the conductivity exponent u is known as $u = \mu/(\mu + s)$ [4, 6].

When both variables, p and h are varied, we can switch from the RRN to the RSN lattice (and vice versa) through the changes $G_A \to 1/G_B$ and $G_B \to 1/G_A$ – or equivalently by interchanging p and q and changing $G_A \to 1/G_A$ and $G_B \to 1/G_B$. When varying the values of the conductances, it is convenient to write $\sigma(p, G_A, G_B)$ as:

$$\sigma(p, G_A, G_B) = G_A\, f(p, h), \tag{2}$$

where $f(p, h)$ is a function for which a well-known scaling behavior applies [4, 6] when p is close to p_c. This connects the conductivity of the RRN and the RSN case:

$$f(p, h) = h\, f(1 - p, h^{-1}). \tag{3}$$

Further insight into the scaling behavior of σ and D can be gained by defining the so-called "dual lattice" $\tilde{L}$ to a given lattice L as e.g. for the case of the honeycomb and the triangular lattices, which are dual to each other. For our purposes, we follow the definitions of [4, 5] for planar lattices without crossing bonds, while more general aspects of dual graphs are found in [15]. Every Archimedean lattice possesses a dual lattice, also called Laves lattice. The geometrical construction of $\tilde{L}$ from L is demonstrated in Fig. 1(i): Considering e.g. the triangular lattice as L, the black lines represent bonds and always three bonds surround one "face" of L. When we cross all bonds between adjacent faces, we arrive at the gray lines that form the bonds of $\tilde{L}$ ("dual bonds"). The crossing points of the dual bonds represent the sites of $\tilde{L}$ ("dual sites"). As we can see in Fig. 1(i), a site of $\tilde{L}$ corresponds to each face of L, while to each bond G corresponds a dual bond $\tilde{G}$. Bonds and dual bonds G and $\tilde{G}$ cross each other, while the dual sites lie inside the faces of L and vice versa. A special case is the square lattice that is self-dual, i.e. its own dual lattice.

With the help of Kirchhoff's laws on L and $\tilde{L}$, it was shown in [5] that $\sigma(p, G_A, G_B) = G_A G_B/\tilde{\sigma}(q, G_A, G_B)$. Moreover, by combining this finding with Eqs. (2) and (3), one arrives at the "reciprocity formula" [4] $\sigma(p, G_A, G_B)\, \tilde{\sigma}(p, G_A^{-1}, G_B^{-1}) = 1$. We keep in mind that the derivation was restricted to planar two-dimensional lattices with non-crossing bonds.

To avoid confusion, we must distinguish between the conductivity $\tilde{\sigma}(p, G_A, G_B)$ of the geometrically dual lattice $\tilde{L}$, and the more important quantity $\tilde{\sigma}(p, G_A^{-1}, G_B^{-1})$ of the "electrical dual lattice", where each conductance $\tilde{G}$ of $\tilde{L}$ has been chosen as the reciprocal conductance $1/G$ of the respective bond of L [4]. The definitions given above do not imply a special angle between bond and dual bond, but in this work, we will always choose them perpendicular to each other. Note that the definition of the electrical dual does not depend on this special choice (provided that the resistance of a bond does not depend on shape and length).

In this work, we consider D instead of σ. In this case, the critical exponents μ and s must be replaced by μ' and s', respectively (while u stays the same). Under the assumption that the densities of charge carriers of L and $\tilde{L}$ are proportional to each other, the same relations as for σ should also apply for the diffusion coefficients D and $\tilde{D}$ of L and $\tilde{L}$, respectively, i.e.

$$D(p, G_A, G_B) = G_A G_B/\tilde{D}(q, G_A, G_B), \tag{4}$$

and

$$D(p, G_A, G_B)\tilde{D}(p, G_A^{-1}, G_B^{-1}) = 1, \tag{5}$$

where $\tilde{D}$ is the diffusion coefficient of the respective reciprocal lattice. A numerical test of Eq. (4) for some selected pairs of Archimedean lattices and their dual lattices in the case $G_A = 1$ is shown in Fig. 2 (see below). Eq. (4) offers several valuable insights that can be found in some detail in [4] (and references therein). As an example, one finds $p_c = 1/2$ for the square lattice from equations (3) and (5) together with $L = \tilde{L}$ (self-duality of the square lattice), as well as characteristic relationships between the values of p_c of any couple L and $\tilde{L}$ [5]. As the RRN lattice transforms to the RSN lattice by replacing G_A by G_A^{-1}, G_B by G_B^{-1} and p with q, one can also argue that $\mu = s$ for the square lattice and therefore $u = 1/2$ [4]. As the critical exponents μ, s (and therefore also u) are assumed universal, $u = 1/2$ should apply for all lattices in $d = 2$. We verify this universality hypothesis for the class of Archimedean lattices in this work by numerical simulations. In $d = 3$, numerical simulations on (small) cubic lattices have shown that $u = 0.72 \pm 0.02$ [5]. It is an interesting question with applications to real materials if u is still universal for lattices that are non-planar and eventually do not have a dual lattice $\tilde{L}$. We will consider some of these cases in the last section.

III. NUMERICAL SIMULATIONS

It is by several reasons preferable to store only those lattice sites and bonds where the walker actually steps to, i.e. to create the lattice during the walk process. This avoids the storage of huge and unnecessary lattice information and enables a walk on a truly infinite system without any danger that the walker touches a predetermined boundary, thereby enforcing an upper limit to the number of time steps. Therefore we decided to use a balanced binary search tree structure, called red-black tree [16] to create the lattice.

The (binary) lattice itself is given by its sites (labeled by i) with nearest-neighbor sites j, the distances a_{ij} and the microscopic resistances $R_{ij} = G_{ij}^{-1}$ between the nearest neighbors, where in our case, all $R_{ij} > 0$. The a_{ij} are identical in an Archimedean lattice, but may have different values in the dual lattices. Here, we follow the lines of [4] and consider the values of the G_{ij} as length-independent, i.e. we attribute constant values G_A or G_B to the bonds, independently of their lengths. This assumption refers e.g. to electrical networks, where the

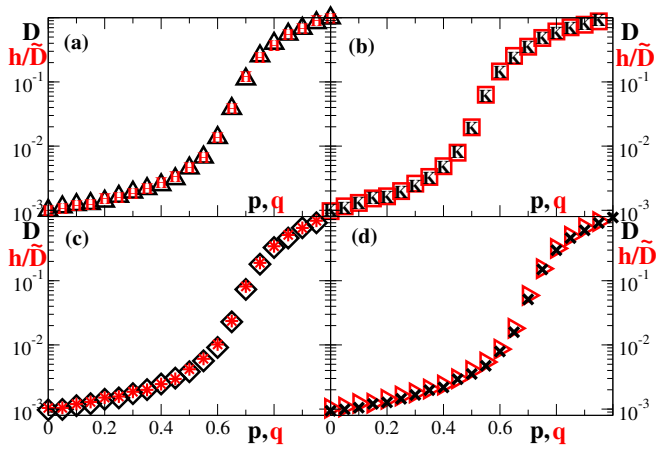

FIG. 2: [Color online] Test of Eq. (4): The diffusion coefficients $D(p, G_A, G_B)$ with $h = G_B/G_A = 10^{-3}$ and $G_A = 1$ of different Archimedean lattices L are plotted versus p (black symbols), while $G_A G_B/\tilde{D}(q, G_A, G_B)$ of the corresponding dual lattices $\tilde{L}$ are plotted versus $q = 1 - p$ (red symbols). The $L/\tilde{L}$ pairs are: (a) Honeycomb/Triangle, (b) Kagome/ Dual of Kagome ("Dice"), (c) Square octagon/Dual of Square octagon, (d) Cross/ Dual of Cross. ($\tilde{L}$ of (b)-(d) are no Archimedean lattices.) The results have been simulated over 10^8 time steps and are averaged over 10^3 runs.

resistances are considered as fixed devices on wires of zero resistance. (A different point of view, with e.g. $G_{ij} \propto a_{ij}^{-1}$ would also be possible).

To perform the random walks of the type "blind ant" [2], we translated the values of G_{ij} and a_{ij} into jump probabilities p_{ij}. For non-blind walks, we also need the mean jump times. While a blind ant chooses one of the possible directions with equal probabilities and may simply wait if the chosen bond is of low conductivity, the non-blind walker jumps in any case, but the jump-times are chosen such that waiting times are implicitly included. We imagine that the walker is at site i with k existing conducting bonds of (normally different) lengths a_{ij} to neighboring places j with $j \in \{1, \ldots, k\}$. The jump probabilities are the normalized conductances, $p_{ij} = G_{ij}/\sum_{j=1}^{k} G_{ij}$. If all bonds have the same lengths, this is sufficient to perform blind walks, otherwise we can at least cut the bonds a_{ij} into smaller "virtual" bonds of roughly the same lengths, where, however, the latter possibility is quite time-consuming and therefore only suited for tests.

To perform (faster) non-blind walks, we can use the virtual bonds as a picture to find the appropriate jump times. In a non-blind walk, the walker chooses one of the directions according to p_{ij}, and performs a jump to site j. Without other neighbor sites, the average time for this jump, according to Fick's law would be (apart from constant factors that we set to unity) $\langle t_{ij} \rangle = a_{ij}^2/G_{ij}$ and represents the time the walker would need to reach the neighbor site j by a random walk over all virtual bonds between sites i and j – including all intermediate returns to i. However, if we have more than one nearest neighbor, we must also take into account that the walker, before having reached j, might step back to i and head for another neighbor site afterwards. This way, the times for jumps from site i to all nearest neighbors are no longer separated from each other but coupled by these failed attempts, so that $\langle t_{ij} \rangle$ must be replaced by the average time over all attempts to leave i, $\langle t_i \rangle = \sum_{j=1}^{k} p_{ij} \langle t_{ij} \rangle = \sum_{j=1}^{k} a_{ij} / \sum_{j=1}^{k} G_{ij}$, with p_{ij} and $\langle t_{ij} \rangle$ from above. This way, we can attribute a mean jump time $\langle t_i \rangle$ to each lattice site. The virtual bonds can now be dropped by performing a non-blind walk from site to site by using only p_{ij} and $\langle t_i \rangle$.

For test purposes, we realized both, "blind" walks over many virtual bonds of roughly equal sub-segments and "non-blind walks". We verified that in all test walks, both procedures lead to the same results for $\langle r^2(t) \rangle$. The numerical results of this work on systems with bonds of unequal lengths are gained on non-blind walks with the appropriate values of p_{ij} and $\langle t_i \rangle$ as described above.

IV. ARCHIMEDEAN LATTICES

We test the relations of paragraph II on the Archimedean lattices and their duals. Some of the duals have bonds of equal lengths, while most have different bond lengths. We consider both cases separately in the following. We start with Eq. (4). (i) Apart from the square lattice (for which relation (4) is trivial because of the self-duality), there are four Archimedean lattices, where also the dual lattices possess only one bond length. We tested them all and found that all fulfill Eq. (4) perfectly. As an example, the results for the lattices of Fig. (1)(d) and (i) are shown in Fig. 2(a,b), where we plot D versus p (black symbols) and $h/\tilde{D}$ versus $q = 1-p$ (red symbols) for $h = 10^{-3}$ and $G_A = 1$. It can be seen that the symbols of both curves lie perfectly upon each other. (ii) In the case of non-equal bond-lengths of the dual lattices, the test of relation (4) is also a sensible test for the chosen values of the p_{ij} and $\langle t_i \rangle$ (see preceding section). As an example, in Figs. 2(c,d), we show the results of the systems of Fig. 1(b) and (c) together with their dual counterparts. Also here, the agreement between both curves is very good.

Next, in Fig. 3, we test the value of the exponent u by plotting D versus h for all Archimedean lattices at their individual values of p_c (taken from Refs. [13, 14]) in a double-logarithmic plot. Indeed, as one would expect from Eq. (1), all curves form straight lines of slope u, that is very close to the expected value of $u = 1/2$. Finally, we test the scaling relation of the binary RRN model [6]

$$D(p, h)/h^u = \Phi_L\left((p - p_c)/h^{u/\mu'}\right). \qquad (6)$$

Here, $\Phi_L(x)$ is a scaling function that depends on the scaling variable $x = (p - p_c)/h^{u/\mu'}$, while the lattice geometry L enters as a parameter. Therefore, a test of the

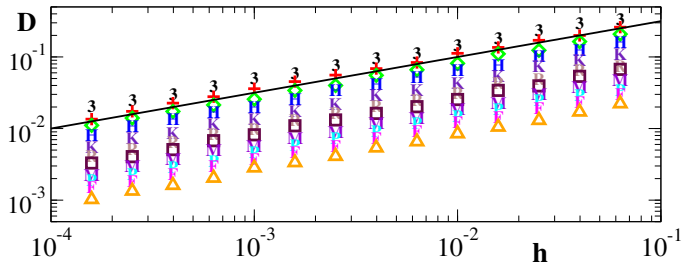

FIG. 3: [Color online] (a) The diffusion coefficient D is plotted at the respective values of p_c versus h for the Archimedean lattices of Fig. 1 (for the symbols see table I). The straight line of slope 1/2 is a guide to the eye. (For clarity reasons, the curves for the individual lattices are shifted into the positive y-direction by multiples of 1.25). Each point corresponds to the average of 1000 random-walks after a simulation time of $t = 10^8$.

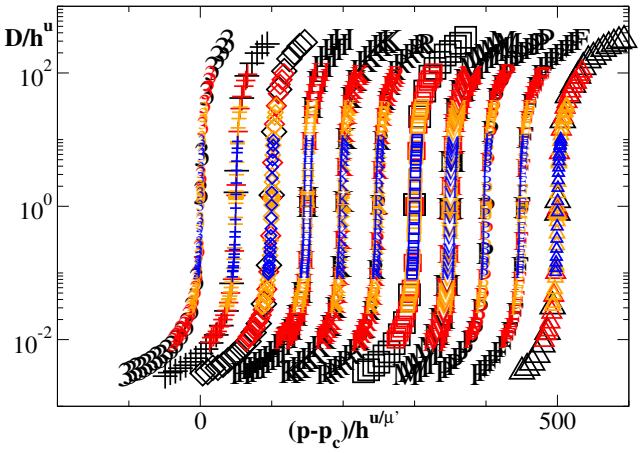

FIG. 4: [Color online] $\Phi_L = D/h^u$ (with $u = 1/2$) is plotted versus $x = (p-p_c)/h^{u/\mu'}$ for the 11 Archimedean lattices, for many different values of p and h. Each symbol corresponds to a different lattice L, as indicated in table I. The data points for each lattice collapse perfectly to a common scaling function $\Phi_L(x)$, thereby confirming the universality hypothesis for the exponent u. The characteristics of these functions in three limited cases are shown in table I. For clarity reasons, the curves for the individual lattices are shifted into the positive x-direction by intervals of 50. The color indicates the value of h: $h = 10^{-2}$ (blue), $h = 10^{-3}$ (orange), $h = 10^{-4}$ (red) and $h = 10^{-5}$ (black). Each point corresponds to the average of 1000 random-walks after a simulation time of $t = 10^8$.

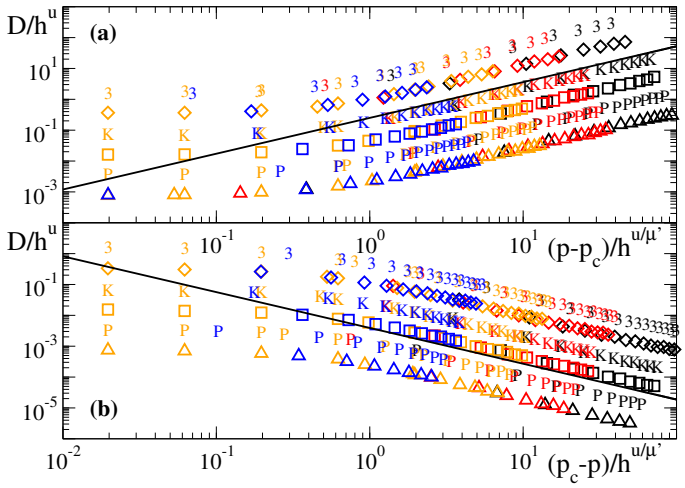

FIG. 5: [Color online] Some of the scaling functions of Fig. 4 are shown in a magnified scale in a double-logarithmic plot. (a) zoom of Φ_L versus $(p-p_c)/h^{u/\mu'}$ in the region $p > p_c$ where the asymptotic exponent is $\mu' \approx 1.16$. (b): zoom of Φ_L versus $(p_c-p)/h^{u/\mu'}$ in the region $p < p_c$ where the asymptotic exponent is $-s' \approx -1.16$. Note that p *decreases* from left to right in this subfigure. (a) and (b): Colors and symbols are the same as in Fig. 4. For clarity reasons, the curves are shifted into the positive y-direction by multiples of 4. The straight lines are guide for the eyes with slopes of ± 1.16.

scaling behavior offers a sensible test, not only for the universality of the exponent u, but also for μ' (and the scaling ansatz itself). In the literature, we found numerical verifications of this relation for the square lattice [6], but to the best of our knowledge, this scaling relation has not yet been tested for the different geometries of Fig. 1.

In Fig. 4, we plot $\Phi_L = D/h^u$ versus $x = (p-p_c)/h^{u/\mu'}$ for all Archimedean lattices of Fig. 1 and for many (positive and negative) values of $p - p_c$ and many values of h with $0 < h \ll 1$ (in a half-logarithmic plot). For clarity reasons, the curves for the different lattices are shifted to the right (otherwise they overlap, even if not being identical). For each lattice L, the data points (same symbol but different colors) collapse perfectly to the corresponding scaling function $\Phi_L(x)$.

At the left and the right ends of $\Phi_L(x)$ one can observe a power-law behavior that we demonstrate in Figs. 5(a,b) in double-logarithmic plots. Figure 5(a) shows the "right ends" of the scaling functions, i.e. the regimes of $x > 0$, while Figure 5(b) shows the "left ends" ($x < 0$). Due to the logarithmic scale the argument is $x = |p-p_c|/h^{u/\mu'}$. Note, that in the following discussion, where we compare the values of h and $|p-p_c|$, the scaling ansatz implies that they both have rather small values. For large values of $|p-p_c|$, we are too far from the percolation threshold, whereas for large values of h, G_B is approaching G_A, so that the percolation threshold becomes invisible. In both cases, only normal diffusion behavior is possible.

(i) The regime $x \gg 1$ (right ends in Fig. 4) is reached for $p > p_c$ and for especially small values of h. In this case, the scaling behavior (6) leads to the power-law $\Phi_L(x) = A_L^+ x^{\mu'}$ with constant A_L^+ (see Fig. 5(a)). A similar diffusion behavior is also observed for standard percolation, i.e. for a system where $h = 0$. This can be interpreted such that the G_B-bonds are nearly not used by the random walker (because of the extremely small jump probabilities), so that its behavior is basically de-

TABLE I: The proportionality constants A_L^+, A_L^- and $\Phi_L(0)$ of the limiting cases of $\Phi_L(x)$ (see text) for each of the 11 Archimedean lattices as well as for the systems with crossing bonds (see next section) are shown together with the corresponding symbols used in all figures.

Lattice	A_L^+	A_L^-	$\Phi_L(0)$	Symb.
3-12	4.5 ± 0.24	0.62 ± 0.03	1.49 ± 0.06	3
Cross	3.83 ± 0.18	0.57 ± 0.03	1.36 ± 0.04	+
Squ. octagon	3.65 ± 0.16	0.57 ± 0.03	1.31 ± 0.04	◇
Honeycomb	3.47 ± 0.14	0.55 ± 0.03	1.27 ± 0.03	H
Kagome	2.54 ± 0.14	0.46 ± 0.02	1.08 ± 0.03	K
Rhombitrihex.	2.35 ± 0.12	0.43 ± 0.02	0.98 ± 0.03	R
Square	2.37 ± 0.1	0.43 ± 0.02	1.0 ± 0.02	□
Snub hex.	2.02 ± 0.14	0.35 ± 0.02	0.89 ± 0.03	M
Snub squ.	2.03 ± 0.1	0.35 ± 0.02	0.87 ± 0.02	P
Frieze	1.98 ± 0.1	0.34 ± 0.02	0.87 ± 0.02	F
Triangular	1.84 ± 0.1	0.29 ± 0.02	0.78 ± 0.02	△
Crossings A	1.82 ± 0.06	0.32 ± 0.02	0.75 ± 0.03	A
Crossings B	2.11 ± 0.09	0.38 ± 0.03	0.83 ± 0.04	B
Two layers	1.43 ± 0.05	0.24 ± 0.02	0.58 ± 0.03	2

termined by the changes of p.

(ii) The regime $x \ll -1$ (left ends in Fig. 4) is a very interesting case, as it does not exist in standard percolation. (For $p < p_c$ and $h = 0$, the walker is trapped in finite clusters.) Here, Eqs. (3) and (6) lead to $\Phi_L(x) = A_L^- |x|^{-s'}$ with constant A_L^- (see Fig. 5(b)). Indeed, and according to the expected universal behavior of $u = 1/2$, we find that the exponent s' is equal to μ'.

(iii) The regime $|x| \ll 1$ is reached for $p \approx p_c$, i.e. for especially small distances of the system from the percolation threshold. In this case $\Phi_L(x)$ tends towards a constant $\Phi_L(0)$, which is consistent with $D = \Phi_L(0) \cdot h^u$ (see Fig. 3). This means that the scaling behavior is basically determined by the changes of h and is similar to the case of Fig. 3.

We find the values of μ' and $-s'$ in the slopes of the two regimes shown in Fig. 5(a) and (b), respectively. In very good accuracy, we find $\mu' = s' \approx 1.16$ and thus $u = 1/2$. The constants A_L^+, A_L^- and $\Phi_L(0)$ were determined numerically: A_L^+ and A_L^- through a least-square fit for the points of Fig. 4 with $|x| > 2$ by assuming that $\mu' = s' = 1.16$; $\Phi_L(0)$ through a least-square fit for the points of Fig. 3 by assuming $u = 1/2$. They are shown in Tab. I. In summary, Figs. 2-5 together give a very good numerical proof of the universality of μ', s' and u for the considered lattices that comprise Archimedean lattices and their duals.

V. LAYERS OF FINITE THICKNESS

In real materials, the surfaces usually do not form perfect planar two-dimensional lattices, but are reconstructed, possibly with crossing bonds. Additionally, in many situations, as e.g. in the gas-exposed surfaces described in the introduction, probably more than one layer of atoms is involved. Layers of finite thickness lie between two- and three-dimensional systems and are therefore not in the same universality class as the systems of Fig. 1.

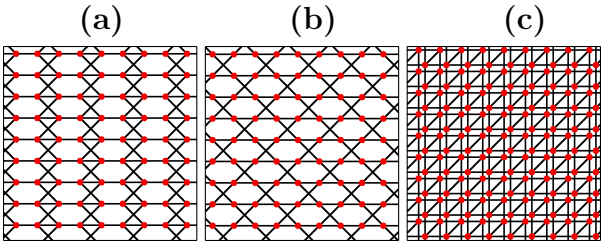

FIG. 6: Systems that we consider in this work. Lattice points are indicated by red dots and bonds are symbolized by black lines that are isolated against each other, so that crossing lines have no electrical or diffusional contact to each other. (a), (b): Variations of the square lattice geometry with "crossing bonds". (c): Two-layer cubic geometry. This geometry can be reduced to a 2D geometry with crossing bonds as explained in the text. We determined the bond percolation thresholds by estimating the proportion of systems having an infinite cluster. By analyzing square systems of side length $2 \cdot 10^4$, we found $p_c^{(A)} = 0.481 \pm 0.0005$ and $p_c^{(B)} = 0.470 \pm 0.0005$. For p_c of the layer system, see Fig. 8.

Layer systems and systems with crossing bonds are related to each other, as we can see in Fig. 6, where we show three systems of this class. Whereas Figs. 6(a,b) (denoted in the following as "crossings A" and "crossings B" – see also Tab. I) are not far from an ordinary two-dimensional system, the system of Fig. 6(c) shows an originally cubic grid consisting of two layers, that we squeezed, so that all bonds are now lying flat inside the xy-plane. The former vertical bonds (into the z-direction) now include an (arbitrary) angle φ to the x-axis (and an angle $\vartheta = \pi/2$ to the z-axis). As a result, a non-planar two-dimensional system is formed with a lot of crossing bonds that we consider as isolated against each other. This example illustrates that systems with crossing bonds are no real two-dimensional systems, but can often be mapped to a layer of two (or more) planes. Therefore, we think that systems with crossing bonds either belong to a different universality class than pure 2D systems, or gradually develop into the class of three-dimensional systems depending on the number of their crossing bonds. This guess is enhanced by the fact that systems with crossing bonds as well as layer systems usually don't possess dual lattices, so that the argument of [5] for the reciprocity formula does not apply to these cases.

We are interested in the diffusion properties of layer systems and systems with crossing bonds. To this end, we performed random walks on the three different systems of Fig. 6 and analyzed them in the same way as the Archimedean lattices. As a test, we tentatively assumed the standard values of the $2D$ exponents u, μ' and s'. In

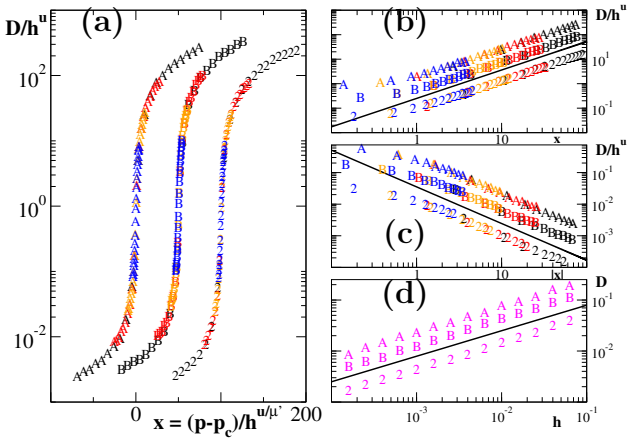

FIG. 7: [Color online] (a) $\Phi = D/h^u$ is plotted versus $x = (p - p_c)/h^{u/\mu'}$ for the lattices of Fig. 6, for many different values of p and h (same colors as in Fig. 4, for symbols see Tab. I). For clarity reasons, the curves are shifted into the (positive) x-direction by intervals of 50. (b,c): zoom of (a) to the regimes $x > 0$ and $x < 0$, respectively, in a double-logarithmic scale (where Φ has been plotted versus $|x|$). The straight lines are guides to the eye with the slope of ± 1.16. For clarity reasons, the curves are shifted into the y-direction by factors of 2. (d): D at criticality is plotted versus h for the lattices of Fig. 6. The line of slope 1/2 is a guide to the eye. The curves with symbols B and 2 are shifted into the negative y-direction by a factor of 2 and 4, respectively. The data have been averaged over 1000 random walks after 10^8 time steps.

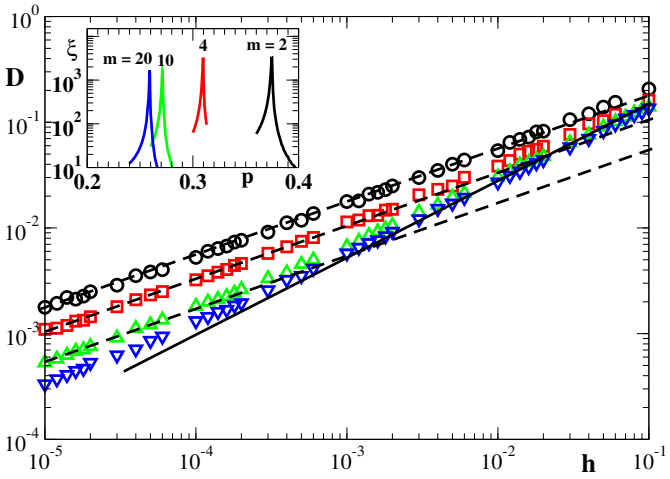

FIG. 8: [Color online] D at p_c is plotted versus h for systems of varying thickness, i.e. for $m = 2$ (black circles), 4 (red squares), 10 (green triangles up) and 20 (blue triangles down) layers, respectively. The dashed lines of slope 0.5 and the full line of slope 0.72 (theoretical values of u in $d = 2$ and $d = 3$, respectively) are guides to the eye. Inset: Correlation lengths ξ of systems with numbers m of layers (as indicated) plotted versus the occupation probability p. The critical concentration p_c is taken from the maximum in ξ, i.e. $p_c = 0.375 \pm 0.001$ for $m = 2$, 0.310 ± 0.001 for $m = 4$, 0.271 ± 0.001 for $m = 10$ and 0.259 ± 0.001 for $m = 20$.

Fig. 7(a), we show the resulting scaling function $\Phi(x)$, whereas Figs. 7(b,c) show the left and the right end of this scaling function in a double-logarithmic plot. Figure 7(d) shows D versus h at criticality in order to find the value of u of these systems. In spite of having used the 2D exponents for these non-planar systems, the results are again surprisingly good and namely the scaling curve still shows a perfect data collapse. Apparently, the crossing bonds don't have a visible effect on the 2D-diffusion behavior yet, which is quite surprising.

In order to find the transition between 2D and 3D, we now increase the number of crossing bonds by investigating layer systems of increasing thicknesses and see in which way the exponents change from 2D to 3D. Squeezing the layer into the xy-plane is unimportant, as the mean squared displacement $\langle r^2_{\rm sqz}(t)\rangle$ of a squeezed layer $\vec{r}_{\rm sqz} = (x + z\cos\varphi, y + z\sin\varphi, 0)$ with the squeezing angle φ as described above is the same as the mean squared displacement $\langle r^2_{3D}(t)\rangle$ of a layer with finite thickness without squeezing, where $\vec{r}_{3D} = (x, y, z)$, i.e. $\langle r^2_{\rm sqz}(t)\rangle = \langle x^2\rangle + \langle y^2\rangle + \langle z^2\rangle + 2\langle xz\rangle\cos\varphi + 2\langle yz\rangle\sin\varphi = \langle x^2 + y^2 + z^2\rangle = \langle r^2_{3D}(t)\rangle$.

The numerical results are shown in Fig. 8 for several layer thicknesses m between 2 and 20 at the percolation threshold. The figure shows $D \equiv \langle r^2_{3D}\rangle/t$ versus h at p_c in a double-logarithmic plot for $h \le 10^{-1}$, i.e. for small h (as the scaling theory breaks down for large h). We took p_c from the maximum in the correlation lengths ξ as shown in the inset. The theoretical curves of $D \propto h^u$ with $u = 0.5$ (2D behavior) and $u = 0.72$ (3D behavior) are shown as dashed and solid lines, respectively. We can see that the curve for $m = 2$ is indeed best described by the exponent $u = 0.5$ in the entire range. This explains the good scaling behavior of Fig. 7 (see above), where the same range of $h \le 10^{-1}$ has been investigated. When increasing the layer thickness m, a 3D behavior ($u = 0.72$) starts to show up at the upper edge, i.e. for larger values of h. For increasing values of m, the range of 3D behavior gradually expands towards smaller values of h. In the system with $m = 20$, the last one that we examined, we found $3D$ behavior for $10^{-1} \ge h \ge 10^{-3}$ (and $2D$ behavior below). Clearly, with an infinite number of layers, a full $3D$-behavior must be reached.

Finally, we want to give a qualitative explanation, why we find the $3D$ behavior at higher and the $2D$ behavior at lower values of h. Imagine first a system at p_c with $h = 0$. In this case, the walker can only follow the paths along the infinite cluster (arranged like a maze), which includes a lot of deviations and dead ends. We now have to distinguish between the "Euclidean distance" r between two sites A and B of the infinite cluster and the "chemical distance" ℓ [1, 2], which measures the length of the path that a walker really has to take by stepping from A to B along G_A-bonds. Two nearest neighbor sites always

have an Euclidean distance of $r = 1$, but may have a very large chemical distance ℓ, when the bond between them is not occupied by a G_A-bond. When the number of layers increases, additional G_A-paths become available between sites A and B that are separated from each other by small distances of r and large distances of ℓ. (This is also the reason why p_c decreases with the number of layers.)

However, chemical paths may be very long (especially in $d = 3$, when they range over many layers) and the diffusion properties are therefore still quite poor at $h = 0$. We think that the effect of the G_B-bonds that leads to Eq. (1) is to build bridges (shortcuts) between long paths of G_A-bonds, so that "mixed paths" of G_A and G_B-bonds arise [17]. It seems reasonable to assume that the more layers a system has (that is, the closer it is to a $3D$-system), the longer the chemical distances can be at p_c. The first reason is the higher number of layers that may extend the paths by simple geometry. Second, the value of p_c decreases with the number of layers, thereby reducing the concentration of sites and thus the crossings between paths, which should also result in longer chemical paths. This is why we think that u, which governs the relation $D \propto h^u$ at $p = p_c$, is bigger in $3D$-systems than in $2D$-systems because of the higher possibility of shortcuts between long G_A-paths in $d = 3$. However, the resulting mixed paths are only important if the probability of being used (that is determined by the jump-probability over a G_B-bond) is big enough as compared to the possibility that the walker steps over the ℓ-path of G_A-bonds instead. This means that at small values of G_B (and thus h), only shortcuts between very long distances ℓ would play a role – which are not present in finite layers. For larger values of h, on the other hand, already shortcuts over smaller chemical distances (that appear in systems with few layers) change the diffusion behavior and make the layer system look as a 3D-system. This assumption is supported by Fig. 8, where we can indeed see that the $3D$-value of u can first be seen for higher values of h and extends to smaller values of h when the number of layers (and thus the lengths of the ℓ-paths) increases. The described effect is a finite-size effect and it is interesting to emphasize, that the change from $2D$ to $3D$ behavior arises gradually and not at a well-defined crossover value of h.

VI. SUMMARY AND CONCLUSION

When interpreting experimental phase transitions, as e.g. the transition between the insulating and the conducting phase, it is important to know how to identify the nature of the transition between the different phases even under non-optimal conditions, when e.g. the lattice is disturbed by defects, surface-reconstructions, or layer thicknesses that are neither clear $2D$ nor clear $3D$ systems. In this paper, we first investigated numerically the transition between the insulating and the conducting phase of binary mixtures of Archimedean lattices with two types of conductances G_A and G_B. We found that the theoretical scaling relations and the universal critical exponents are met with very high precision in all the Archimedean lattice structures. Moreover, these laws persist also in square lattices with surface reconstructions in the form of crossing bonds and for a layer of thickness two, where some preconditions of the scaling theory are no longer valid and where the system is no longer a real $2D$ system.

In cases of binary layer systems of cubic lattice structure, we investigated the conductance exponent and found that, at the critical concentration, binary layer systems of cubic lattice structure of higher thicknesses ($m > 3$) show a crossover with $u = 0.72$ at higher and $u = 0.5$ at smaller values of h, that correspond to the value of u in $d = 3$ and $d = 2$, respectively. Experimentally, this means that both values may be found, depending on the different conductances between the lattice sites. We gave a qualitative explanation for the behavior of this crossover.

However, when experimental deviations of the theoretical exponents are reported in binary systems, one should also keep in mind that two parameters are subject to changes: the relation h between the two different interatomic conductances and the concentration p of bonds with the higher conductance. In experimental situations, it may not always be clear if a given external influence (as e.g. the exposure of the system to a certain gas) changes h or p or possibly both. In these situations, the scaling law (6) should be carefully considered.

Additionally, one should keep some idealizations in mind that are normally made in theoretical considerations and simulations (also in this work). For example, we assumed that the concentration of charge carriers n is independent of the number of conducting bonds and that the lattice type is not changed during the transition. As the transition might e.g. be driven by chemical reactions and chemical transformations of the lattice atoms, this might not always be the case. We think that our investigations, even if several open questions still remain, will help in the future to interpret these types of phase transitions.

VII. ACKNOWLEDGEMENTS

We gratefully acknowledge financial support from the Freie Universität Berlin and valuable discussions on the experimental situations with C.-D. Kohl and J. Hennemann.

[1] *Fractals and Disordered Systems*, 2nd ed., edited by A. Bunde and S. Havlin (Springer, Berlin, 1996); D. Stauffer and A. Aharony *Introduction to percolation theory*, 2nd ed., (Taylor and Francis, London, 1994).

[2] D. ben-Avraham and S. Havlin; *Diffusion and Reactions in Fractals and Disordered Systems*,Cambridge University Press, (Cambridge, UK, 2004).

[3] P. Maass, A. Bunde and M. D. Ingram, Phys. Rev. Letts. **68**, (1992) 3064 and A. Bunde, M. Ingram and S. Russ; Phys. Chem. Chem. Phys. **6**, 3663 (2004).

[4] J. P. Clerc, G. Giraud, J. M. Laugier and J. M. Luck; Adv. Phys. **39**, 191 (1990).

[5] J. P. Straley; Phys. Rev. B **15** 5733 (1977).

[6] D. C. Hong, H. E. Stanley, A. Coniglio and A. Bunde; Phys. Rev. B **33** (1986) 4564.

[7] M. Ulrich, A. Bunde, C.-D. Kohl, Appl. Phys. Lett. **85**, 242 (2004).

[8] S. Russ; Phys. Rev. E **90**, 022141 (2014).

[9] T. Sauerwald and S. Russ in *Gas Sensing Fundamentals*, ed. by C.-D. Kohl and T. Wagner; Springer Series on Chemical Sensors and Biosensors

[10] J. Dräger, S. Russ, T. Sauerwald, C.-D. Kohl and A. Bunde; J. Appl. Phys. **113**, 223701 (2013).

[11] J. Hennemann, C.-D. Kohl, B. Smarsly, T. Sauerwald, J.-M. Teissier, S. Russ and T. Wagner; Phys. Status Solidi A, **212**, 1281 (2015).

[12] J. Hennemann, C.-D. Kohl, B. Smarsly, H. Metelmann, M. Rohnke, J. Janek, D. Reppin, B. K. Meyer, S. Russ and T. Wagner; Sens. and Actuators B **217**, 41 (2015) (Springer Verlag Berlin Heidelberg 2013), Doi 10.1007/5346_2013_53.

[13] P. N. Suding and R. M. Ziff; Phys. Rev. E **60**, 275 (1999).

[14] R. Parviainen; J. Phys. A **40**, 9253 (2007).

[15] Thomassen C., Duality of Infinite Graphs, Journal of Combinatorial Theory, Series B **137-160** (1982).

[16] T. H. Cormen, C. E. Leiserson, R. L. Rivest and C. Stein; *Introduction to Algorithms*, 3rd ed., (The MIT Press, 2009).

[17] S. Russ, H. E. Roman and A. Bunde; J. Phys.: Condens. Matter **3** (1991) 4797.